Plenty of Room on the Top: Pathways and Spectroscopic Signatures of Singlet Fission from Upper Singlet States

Yiting Bai,[†] Wenjun Ni,[†] Kewei Sun,[†] Lipeng Chen,[‡] Lin Ma,[¶] Yang Zhao,[§] Gagik G. Gurzadyan,[‖] and Maxim F. Gelin[†]

School of Sciences, Hangzhou Dianzi University, Hangzhou 310018, China , Max-Planck-Institut für Physik komplexer Systeme, Nöthnitzer Strasse 38, D-01187 Dresden, Germany, School of Physics and Optoelectronic Engineering, Guangdong University of Technology, 510006 Guangdong, China, School of Materials Science and Engineering, Nanyang Technological University, Singapore 639798, Singapore, and State Key Laboratory of Fine Chemicals, Institute of Artificial Photosynthesis, Dalian University of Technology, 116024 Dalian, China

E-mail:

Abstract

We investigate dynamic signatures of the singlet fission (SF) process triggered by the excitation of molecular systems to an upper singlet state S_N ($N > 1$) and develop a computational methodology for the simulation of nonlinear spectroscopic signals revealing the $S_N \to TT_1$ SF

*To whom correspondence should be addressed

†School of Sciences, Hangzhou Dianzi University, Hangzhou 310018, China

‡Max-Planck-Institut für Physik komplexer Systeme, Nöthnitzer Strasse 38, D-01187 Dresden, Germany

¶School of Physics and Optoelectronic Engineering, Guangdong University of Technology, 510006 Guangdong, China

§School of Materials Science and Engineering, Nanyang Technological University, Singapore 639798, Singapore

‖State Key Laboratory of Fine Chemicals, Institute of Artificial Photosynthesis, Dalian University of Technology, 116024 Dalian, China

in real time. We demonstrate that SF can proceed directly from the upper state S_N bypassing the lowest excited state S_1. We determine the main $S_N \rightarrow TT_1$ reaction pathways and show, by computer simulation and spectroscopic measurements, that the S_N-initiated SF pathway can be faster and more efficient than the traditionally studied channel of $S_1 \rightarrow TT_1$. We claim that the $S_N \rightarrow TT_1$ SF offers novel promising opportunities for engineering SF systems and enhancing SF yields.

Singlet fission (SF) is a spin-allowed photophysical process discovered over fifty years ago.[1] In SF, a photo-excited singlet electronic or excitonic state generates two correlated (entangled) triplet states.[2–7] SF has received a lot of attention in recent years, thanks to its great potential for enhancing light harvesting, doubling the photovoltaic efficiency and circumventing the Shockley-Queisser limit.[8,9]

Energy conservation implies that SF is efficient if the singlet state energy is approximately twice as large as that of the triplet. Usually, this statement is understood as the restriction imposed on the electronic energies and is written as

$$E_S \approx 2E_T \approx E_{TT} \tag{1}$$

where E_S, E_T, and E_{TT} are electronic energies of the singlet state, triplet state, and correlated triplet pair. Furthermore, the electronic states are customarily understood as the lowest excited electronic states, meaning that $S = S_1$, $T = T_1$, and $TT = TT_1$. Vibrational energies often enters the arguments as an important, but secondary factor. A notable exception is rubrene, for which E_{S_1} is slightly lower that E_{TT_1}, and thermal activation is required to initiate the SF process.[10]

It is essential that vibrational energy plays a pivotal role in the energy balance and transfer, hence a more general variant of Eq. (1) reads

$$E_S + E_S^{(v)} \approx 2(E_T + E_T^{(v)}) \approx E_{TT} + E_{TT}^{(v)} \tag{2}$$

where $E_S^{(v)}$, $E_T^{(v)}$, and $E_{TT}^{(v)}$ are vibrational energies of the singlet state, triplet state, and correlated

triplet pair, respectively. The are no fundamental restrictions on which the singlet excited state is electronically coupled to the triplet pair. Therefore, the requirement of Eq. (2) extends possible SF scenarios considerably. Indeed, the total energy of the initially excited singlet state matches, essentially, the carrier frequency of the pump pulse,

$$E_S + E_S^{(v)} \approx \omega_{pu} \tag{3}$$

($\hbar = 1$). Hence Eq. (2) suggests the existence of SF pathways leading from a higher-lying singlet state S_N to upper vibrational levels of the TT_1 state. This was recognized by Ma, Ni, Gurzadyan and coworkers, who unequivocally demonstrated by direct real-time spectroscopic measurements the presence of $S_N \rightarrow TT_1$ pathways in rubrene crystals [11,12] and films, [13] perylene dimers in solution, [14] crystals [15] and films, [16] as well as in thiophene crystals and films. [17]

The aim of this work is twofold. First, we develop a theoretical framework for the simultaneous description of the $S_1 \rightarrow TT_1$ and $S_N \rightarrow TT_1$ pathways and simulate electronic populations, transient-absorption (TA) pump-probe (PP) signals, and time- and frequency-resolved luminescence (TFRL) spectra which, taken together, provide a fairly comprehensive view of the SF process. Up to now, time-resolved nonlinear spectroscopic signals were simulated with the multidimensional Redfield theory, [18–21] phenomenological master equations, [22–25] the Davydov Ansatz method, [26–31] the *ab initio* parameterized Pariser-Parr-Pople Hamiltonian, [32–35] and the time-dependent density functional theory method, [36,37] but for $S_1 \rightarrow TT_1$ SF systems only. Second, we explore spectroscopic signatures and identify the main pathways of the $S_N \rightarrow TT_1$ SF reaction as well as discuss novel strategies which emerge for optimizing the $S_N \rightarrow TT_1$ SF but are not feasible for the conventional $S_1 \rightarrow TT_1$ SF. In our simulations, we employ a model SF system mimicking rubrene. Our choice is motivated by ample experimental data on rubrene's $S_N \rightarrow TT_1$ SF [11–13] as well as by the high potential of rubrene as a promising material for energy applications. [38,39]

We broadly identify the SF system as a molecular dimer (if SF takes place in the gas phase or in a solvent) or as an effective dimer (if SF takes place in a crystal or film). Then the SF system

Hamiltonian can be defined as

$$H = \begin{pmatrix} H_S & U \\ U & H_{TT} \end{pmatrix}. \tag{4}$$

Here the Hamiltonian H_S contains all relevant singlet states and associated vibrational modes, the Hamiltonian H_{TT} accommodates all necessary correlated triplet pair states and associated vibrational modes, and U is the coupling operator responsible for the $S \rightarrow TT$ SF occurring on a femtosecond timescale. Decomposition of correlated triplet states into uncorrelated triplets, $TT \rightarrow T + T$, occurs on sub-picosecond timescale and is not considered in this work.

In the diabatic electronic representation,

$$H_S = \sum_k |S_k\rangle (h_{S_k} + E_{S_k}) \langle S_k| + \sum_{k \neq l} |S_k\rangle \Delta_{S_k S_l} \langle S_l|, \tag{5}$$

$$H_{TT} = \sum_m |TT_m\rangle (h_{TT_m} + E_{TT_m}) \langle TT_m| + \sum_{m \neq n} |TT_m\rangle \Delta_{TT_m TT_n} \langle TT_n|, \tag{6}$$

$$U = \sum_{kn} |S_k\rangle U_{S_k TT_n} \langle TT_n| + H.c. \tag{7}$$

Here E_{S_k}, h_{S_k} and $\Delta_{S_k S_l}$ are electronic energies, vibrational Hamiltonians, and interstate couplings in the singlet-state manifold, respectively. E_{TT_m}, h_{TT_m} and $\Delta_{TT_m TT_n}$ are electronic energies, vibrational Hamiltonians and interstate couplings in the manifold of correlated triplet states, respectively, and $U_{S_k TT_n}$ are the couplings between the singlet and correlated triplet states.

In the dipole approximation, coupling of the SF system with laser pulses is described by the Hamiltonian

$$H_L(t) = -\boldsymbol{\mu} \cdot \boldsymbol{E}(t) \tag{8}$$

where $\boldsymbol{E}(t)$ is the total electric field,

$$\boldsymbol{\mu} = \begin{pmatrix} \boldsymbol{\mu}_S & 0 \\ 0 & \boldsymbol{\mu}_{TT} \end{pmatrix}$$

is the transition dipole moment (TDM) operator of the SF system, and $\boldsymbol{\mu}_S$ ($\boldsymbol{\mu}_{TT}$) describe electronic

transitions within the S (TT) manifolds.

Vibrational degrees of freedom of the SF system which are not included in the system Hamiltonian H as well as degrees of freedom of the solvent or crystal/film are considered as the dissipative environment and treated with the master equation for the reduced (system) density matrix $\rho(t)$[40]

$$\partial_t \rho(t) = -i[H + H_L(t), \rho(t)] - (\mathscr{R} + \mathscr{D})\rho(t). \tag{9}$$

Here the operator $\mathscr{R}$ accounts for vibrational relaxation in the manifolds of singlet and triplet sates, while $\mathscr{D}$ describes electronic dephasing.

Numerical solution of the master equation (9) in combination with the so-called spectroscopic equation-of-motion methods of Refs.[41,42] yields TA PP signals $I_{PP}(t,\omega)$ and TFRL spectra $I_{LU}(t,\omega)$ for any H, $\boldsymbol{\mu}$ and $\mathscr{R}$. In the present work, we adopt the vibronic coupling (VC) representation of the system Hamiltonian H which is widely used for the construction of Hamiltonians of chromophores,[43,44] molecular aggregates,[45] and molecular materials.[46] To have a clear picture of the $S_1 \to TT_1$ and $S_N \to TT_1$ SF processes, we include the minimal number of relevant electronic states and vibrational modes and consider four singlet states, two correlated triplet states, and a single vibrational mode. The singlet states include the ground state S_0, the lowest excited state S_1, an intermediate excited state S_M and an upper state S_N. The singlet states are coupled through the constants $U_{S_N S_M}$ and $U_{S_M S_1}$ which are responsible for the downhill $S_N \to S_M \to S_1$ internal conversion. The lowest excited triplet state TT_1 and an upper triplet state TT_M are assumed to be decoupled from each other. The coupling between the manifolds of the singlet and triplet states is governed by the constants $U_{S_1 TT_1}$ and $U_{S_N TT_1}$ which are responsible for the $S_1 \to TT_1$ and $S_N \to TT_1$ SF. Other excited electronic states which may contribute to the SF process (e.g., charge-transfer states and doubly-excited sates[30,31,47–51]) are not considered in the present work but can be readily included if necessary. Vibrational Hamiltonians include a primary vibration mode with frequency Ω, and dimensionless momentum P and position Q:

$$h_{S_k} = \frac{\Omega}{2}\left(P^2 + (Q - \overline{Q}_{S_k})^2\right), \tag{10}$$

$$h_{TT_m} = \frac{\Omega}{2}\left(P^2 + (Q - \overline{Q}_{TT_m})^2\right) \tag{11}$$

(more modes can be included if necessary). Here $\overline{Q}_{S_k}$ and $\overline{Q}_{TT_m}$ are dimensionless displacements of the potential energy surfaces (PESs) of the excited singlet and triplet states from the ground state S_0 ($\overline{Q}_{S_0} = 0$). We chose the vibrational parameters mimicking those of rubrene and set $\Omega = 1500\,\mathrm{cm}^{-1} = 0.186$ eV (the vibrational period $\tau^{\Omega} = 2\pi/\Omega = 22$ fs), $\overline{Q}_{S_1} = -2$ and $\overline{Q}_{TT_1} = 2$ (cf. Refs.[10,27–30]). Since no information about PESs of rubrene's singlet and triplet states in the vicinity of $250\,\mathrm{nm} = 4.96$ eV is available in the literature, we set $\overline{Q}_{S_M} = 2$, $\overline{Q}_{S_N} = -2.25$, and $\overline{Q}_{TT_M} = 2$ (the chosen values allow us to reproduce the experimental TA PP signals, see below). The corresponding singlet (solid lines) and triplet (dashed lines) PESs are schematically shown in Fig. 1.

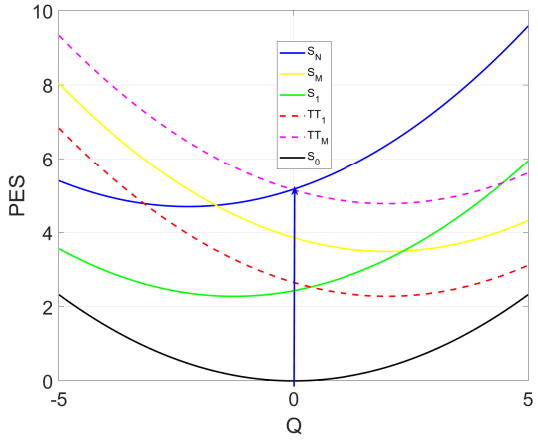

Figure 1: Schematic view of the PESs of the SF model.

TDMs of the present SF model can be decomposed into the lowering and raising components, $\boldsymbol{\mu} = \boldsymbol{X} + \boldsymbol{X}^{\dagger}$, where

$$\boldsymbol{X} = \boldsymbol{\mu}_{S_0S_1}|S_0\rangle\langle S_1| + \boldsymbol{\mu}_{S_0S_M}|S_0\rangle\langle S_M| + \boldsymbol{\mu}_{S_0S_N}|S_0\rangle\langle S_N| + \boldsymbol{\mu}_{TT_1TT_M}|TT_1\rangle\langle TT_M|. \tag{12}$$

The first three terms in Eq. (12) describe transitions within the manifold of singlet electronic states, responsible for ground-state bleach (GSB) and stimulated emission (SE) contributions to

the TA PP signal, while the last term describes transitions between the triplet states TT_1 and TT_M, yielding the excited-state absorption (ESA) contribution. For simplicity, all TDMs are treated as scalar coupling coefficients $\mu_{kn} = \boldsymbol{e}\boldsymbol{\mu}_{kn}$, where $\boldsymbol{e}$ is the unit vector of the polarization of the laser pulses. If necessary, the vector character of TDMs can be taken care of, and orientational averaging can be performed according to Ref.[52]

Dissipation operator $\mathscr{R}$ in Eq. (9) is treated with the multilevel Redfield theory[53] by adopting the representation of Pollard and Friesner[54] and using the Ohmic bath spectral density with exponential cutoff, $g(\omega) = \eta\omega\exp(-\omega/\Omega)$, η being the dimensionless parameter quantifying the system-environment coupling (see Ref.[55] for technical details). For the present class of system Hamiltonians, Redfield theory is an accurate and reliable simulation tool in the weak coupling regime ($\eta \ll 1$).[55,56] Master equation (9) is integrated numerically with the fourth-order Runge-Kutta method, and TA PP signals $I_{PP}(t,\omega)$ as well as TFRL spectra $I_{LU}(t,\omega)$ are evaluated by the spectroscopic equation-of-motion method of Refs.[41,42] TA PP signals are computed for 20 fs Gaussian pump and probe pulses, while TFRL spectra are obtained for 20 fs Gaussian pump pulse and 50 fs time-resolution of the up-conversion setup.

To elucidate the main microscopic mechanisms governing SF from upper sates, it is insightful to consider the coupled $S_N - TT_1$ pair in isolation from other states and monitor the triplet state population, $P_{TT_1}(t)$, after the instantaneous $S_0 \rightarrow S_N$ excitation. The $S_N - TT_1$ population transfer is determined, primarily, by the following four factors (cf. Refs.[57,58]): (a) interstate coupling constant $U_{S_NTT_1}$, (b) system-environment coupling η, (c) $S_N - TT_1$ vibrational level alignment, and (d) $S_N - TT_1$ energy gap $\Delta_E = E_{S_N} - E_{TT_1}$. The impact of these four factors is exemplified by panels (a)-(d) of Fig. 2.

We start from the general description of the population dynamics in Fig. 2. Obviously, $P_{TT_1}(0) = 0$ since the SF system is initially prepared in the optically bright S_N state. The short-time $P_{TT_1}(t)$ evolution is characterized by the step-like population increase, which reveals periodic ($\tau^{\Omega} = 22$ fs) $S_N \leftrightarrow TT_1$ excursions of the vibrational wavepacket (vibrational signatures in spectroscopic responses of various $S_1 - TT_1$ SF systems are discussed in Refs.[59–64] and review[65]). At longer

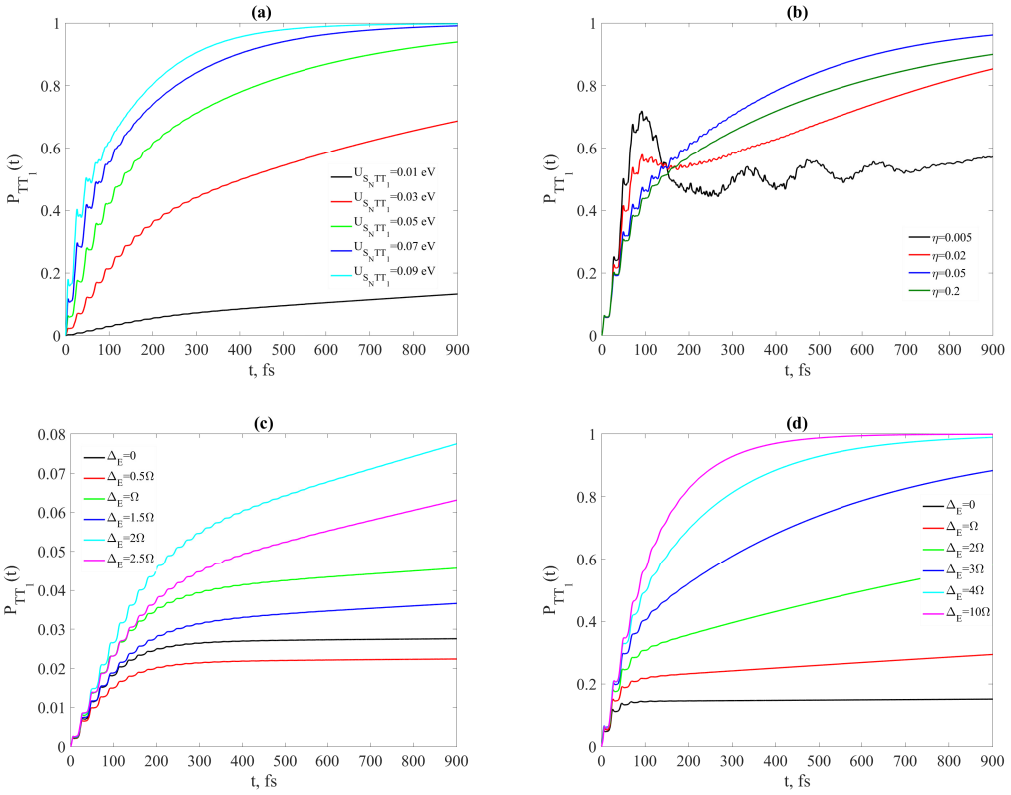

Figure 2: Time evolution of the population $P_{TT_1}(t)$ for different (a) $S_N - TT_1$ couplings $U_{S_NTT_1}$, (b) system-environment couplings η, (c) $S_N - TT_1$ vibrational level alignments, and (d) $S_N - TT_1$ energy gaps Δ_E.

times, $P_{TT_1}(t)$ attains a steady-state value that depends on the system parameters. $P_{TT_1}(t)$ in Fig. 2 do not exhibit a simple exponential rise and therefore the $S_N - TT_1$ SF cannot be treated as a rate process. This is one of the facets of the vibronic wavepacket picture of internal conversion,[66] all dynamical aspects of which are determined by geometry of the corresponding PESs and by the initial wavepacket placement. The SF system of Fig. 1 has a large energy gap Δ_E between the S_N and TT_1 states, and PESs of these states cross substantially below the Franck-Condon region indicated by the blue arrow. Hence the $S_N \to TT_1$ process is controlled by the ballistic downhill wavepacket motion, which renders the SF efficient and fast.

Let us now examine how $P_{TT_1}(t)$ depends on specific SF-governing parameters. Fig. 2(a) illustrates the influence of the $S_N - TT_1$ coupling. $P_{TT_1}(t)$ are plotted for $\Delta_E = 3\Omega$ and $\eta = 0.1$ for several values of $U_{S_NTT_1}$ indicated in the legend. For the smallest $U_{S_NTT_1}$ (black line) the $S_N - TT_1$ population transfer can be approximately described by Fermi's golden rule with the rate $\sim U^2_{S_NTT_1}$. For stronger couplings, the transfer is governed by the two-stage evolution process. The first, faster stage is characterized by a series of population transfers and forward-backward wavepacket excursions in the coupled $S_N - TT_1$ PESs accompanied by vibrational energy relaxation and cooling. The second, slower stage involves the population transfer of the vibrationally cooled wavepacket at energies in the vicinity of the PESs crossing. Increasing $U_{S_NTT_1}$ facilitates SF, and full $S_N - TT_1$ population transfer is achieved on a ~ 1 ps timescale with two largest values of $U_{S_NTT_1}$.

Fig. 2(b) examines the impact of the environment-induced vibrational relaxation. Shown are $P_{TT_1}(t)$ for $\Delta_E = 3\Omega$ and $U_{S_NTT_1} = 0.05$ eV for several system-environment coupling strengths η indicated in the legend. For the smallest η (black line), $P_{TT_1}(t)$ exhibits a series of large-amplitude population recurrences with a period of ~ 150 fs. These recurrences are attributed to synchronization of the vibrational dynamics of the mode Ω with electronic dynamics specified by (vibrationally-renormalized) Rabi frequency $\Omega_R \sim U_{S_NTT_1}$. A recent discussion of vibronic recurrences and their spectroscopic signatures can be found in Ref.[67] Increasing η suppresses the recurrences, makes the $S_N - TT_1$ population transfer irreversible and thereby facilitates SF.

Fig. 2(c) demonstrates the impact of vibrational level alignment. It shows $P_{TT_1}(t, \Delta_E)$ (the

explicit dependence on the energy gap Δ_E is indicated to facilitate the upcoming discussion) for $U_{S_N TT_1} = 0.01$ eV, $\eta = 0.1$ and $\Delta_E = 0.5\Omega j$ ($j = 0,1,2,3,4,5$). For even j, Δ_E accommodates an integer number of Ω, which corresponds to perfectly aligned vibrational levels of the S_N and TT_1 states. For odd j, vibrational levels of the S_N and TT_1 states are shifted by 0.5Ω and are maximally misaligned. Owing to this effect, populations for different Δ_E are arranged in zigzag manner: $P_{TT_1}(t,\Omega/2) < P_{TT_1}(t,0) < P_{TT_1}(t,3\Omega/2) < P_{TT_1}(t,\Omega) < P_{TT_1}(t,5\Omega/2) < P_{TT_1}(t,2\Omega)$. This is caused by resonant effects: for weaker $U_{S_N TT_1}$, the population transfer in the aligned system is more efficient.

Fig. 2(d) also displays $P_{TT_1}(t,\Delta_E)$ for increasing energy gaps Δ_E, but for larger $U_{S_N TT_1} = 0.05$ eV and stronger dissipation $\eta = 0.3$. In this situation, notably for large Δ_E, the level alignment loses its significance. The SF efficiency increases with Δ_E and, for $\Delta_E = 10\Omega$ (pink line), a complete population transfer occurs around $t = 500$ fs. The physical mechanism behind the efficient population transfer at large Δ_E has already been discussed: if the Franck-Condon region of the S_N state is above the PESs crossing, then the $S_N \to TT_1$ internal conversion is fast and efficient. This regime is opposite to that described by the celebrated energy gap law which shows that the population transfer rate, evaluated via Fermi's golden rule, the stationary phase approximation and several other approximations, decreases exponentially with the energy gap, $\sim \exp(-\Delta_E/\Omega)$.[68,69]

Having established the main factors responsible for the direct $S_N - TT_1$ SF, we discuss the S_N-excited SF pathways and their spectroscopic signatures. Three major pathways are conceivable: (i) direct $S_N \to TT_1$ SF considered above, (ii) cascading $S_N \to S_M \to S_1 \to TT_1$ SF, and (iii) combination thereof. Electronic populations $P_i(t)$ ($i = S_N, S_M, S_1, S_{TT_1}$) (upper panels) and TFRL spectra (lower panels) for these pathways are shown in Fig. 3. The observables are calculated for electronic energies $E_{S_N} = 4.64$ eV; $E_{S_M} = 3.46$ eV, $E_{S_1} = 2.279$ eV, $E_{TT_1} = 2.28$ eV mimicking those of rubrene (see Fig. 1 and Refs.[10–13]), the environment-induced relaxation is assumed to be moderate ($\eta = 0.3$) and – for convenience of the discussion to follow – all TDM coupling constants are taken the same ($\mu_{S_0 S_N} = \mu_{S_0 S_M} = \mu_{S_0 S_1} = 1$). The SF is triggered by a 20 fs 250 nm ($\omega_{pu} = 4.96$ eV) pump pulse arriving at $t = 0$.

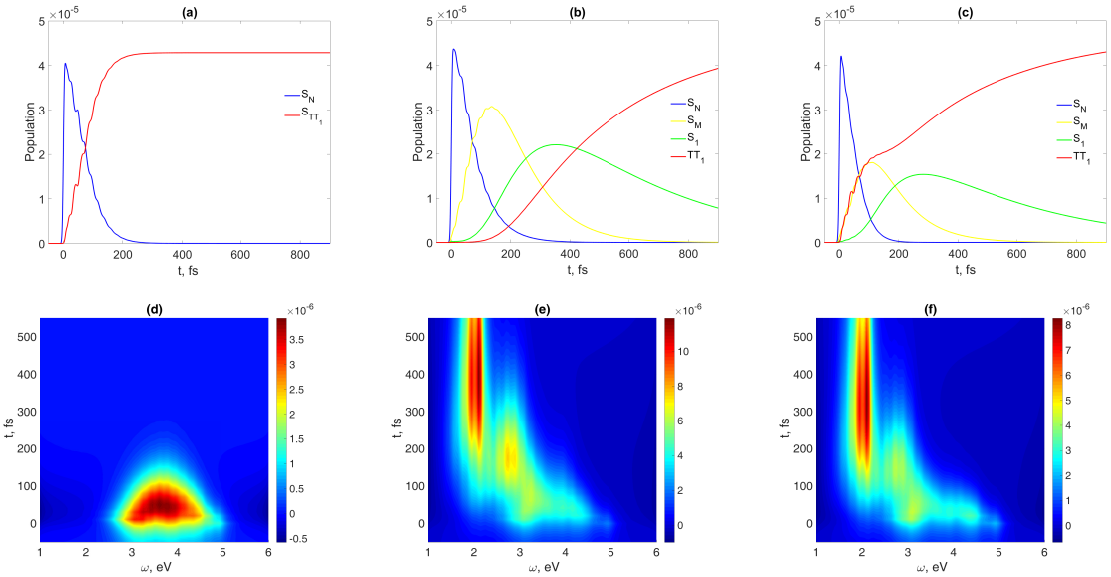

Figure 3: Electronic populations $P_i(t)$ (upper panels) and TFRL spectra $I_{LU}(t,\omega)$ (lower panels) for three different SF pathways: (a,d) direct $S_N \rightarrow TT_1$ SF, (b,e) cascading $S_N \rightarrow S_M \rightarrow S_1 \rightarrow TT_1$ SF, and (c,f) combination thereof.

Figs. 3 (a,d) show populations and TFRL spectrum for direct SF. The $S_N - TT_1$ coupling is relatively strong ($U_{S_N TT_1} = 0.078$ eV), the cascading pathway is switched-off ($U_{S_N S_M} = 0$), and only two states, S_N and TT_1, are involved in SF. Populations (panel (a)) show that SF is complete with a 200% yield on a ~ 250 fs timescale. The same information is illustrated by the TFRL spectrum $I_{LU}(t,\omega)$ (panel (d)). The $S_N \rightarrow S_0$ luminescence starts at $t \approx 0$ in the spectral region $2.7 \leq \omega \leq 4.6$ eV, narrows towards $\omega \approx 3.75$ eV due to vibrational relaxation, and quenches at $t \approx 250$ fs.

Figs. 3 (b,e) explore the cascading leg $S_N \rightarrow S_M \rightarrow S_1 \rightarrow TT_1$ of the SF process. Electronic couplings between the singlet states are moderate ($U_{S_N S_M} = 0.06$ eV, $U_{S_M S_1} = 0.03$ eV), the $S_1 \rightarrow TT_1$ coupling is also moderate ($U_{S_N S_{TT_1}} = 0.04$ eV), and the $S_N \rightarrow TT_1$ pathway is inhibited ($U_{S_N TT_1} = 0$). $P_i(t)$ in panel (b) reveal sequential population transfers $S_N \rightarrow S_M$ at $t \approx 130$ fs, $S_M \rightarrow S_N$ at $t \approx 350$ fs, and the $S_1 \rightarrow TT_1$ SF occurs on a time scale of a few picoseconds. Panel (e) maps this sequence of population transfers onto the TFRL spectrum $I_{LU}(t,\omega)$. Quenching of the S_N luminescence ($2.7 \leq \omega \leq 4.6$ eV) at $t \approx 130$ fs is accompanied by a rise of the S_M luminescence ($2.5 \leq \omega \leq 3$ eV) which vanishes at $t \approx 370$ fs giving birth to the S_1 emission ($1.65 \leq \omega \leq 2.25$

eV) which finally decays on a picosecond timescale owing to the $S_1 \rightarrow TT_1$ SF.

Figs. 3 (c,f) illustrate superposition of the $S_N \rightarrow TT_1$ and $S_N \rightarrow S_M \rightarrow S_1 \rightarrow TT_1$ pathways. According to panel (c), $P_{S_N}(t)$ decays on ~ 100 fs time scale, $P_{S_M}(t)$ reaches its maximum at $t \approx 100$ fs, while $P_{S_1}(t)$ attains its maximum at $t \approx 290$ fs. These time intervals are shorter and the population maxima are lower than those in panel (b). The $P_{TT_1}(t)$ population in panel (c), on the other hand, grows much faster than its counterpart in panel (b), reaching half of its asymptotic value at $t \approx 150$ fs. All these phenomena are promoted by the direct $S_N \rightarrow TT_1$ SF contribution. The TFRL spectrum (panel (f)) reveals the same timescales and processes through luminescence from the S_N, S_M and S_1 states.

Note that the coupling parameters for the system of Fig. 3 were chosen in ad hoc manner just for the sake of argument. We claim, however, that superposition of two or more coherent pathways is ubiquitous in $S_N \rightarrow TT_1$ SF reactions, being thereby a signature of the SF from upper excited states. Indeed, the part $S_N \rightarrow S_M \rightarrow S_1$ of the cascading pathway describes internal conversion to the lowest excited state. This process, according to Kasha's law and Vavilov's rule, is fast and spans hundreds of femtoseconds for most of polyatomic molecular systems.[70] The direct $S_N \rightarrow TT_1$ SF has a comparable or even faster timescale.[11–17] It is therefore highly likely that the direct and cascading SF pathways will compete with each other. This opens up an exciting opportunity of using the coherent control methodology[71] for optimizing SF from upper singlet states. Quantum interference effects in the $S_1 \rightarrow TT_1$ SF were recently discussed in Ref.[72]

Having established the main factors governing the SF from upper states, we simulate the short-time portion of the experimental TA PP signals of rubrene crystal, which monitor the $S_1 \rightarrow TT_1$ and $S_N \rightarrow TT_1$ SF in real time through the $TT_1 \rightarrow TT_M$ ESA.[73] As has been established in Ref.[10] the $S_1 \rightarrow TT_1$ SF is controlled by the conical intersection. Since no information about topology of the S_N and TT_1 PESs in the vicinity of their crossing is available, we prefer to describe both $S_1 \rightarrow TT_1$ and $S_N \rightarrow TT_1$ SF processes in terms of phenomenological coupling coefficients of Eq. (7) assuming the direct SF scenario. The best-fit values of the parameters are found as follows: $U_{S_1TT_1} = 0.0135$ eV, $\eta = 0.06$ ($S_1 \rightarrow TT_1$) and $U_{S_1TT_1} = 0.0208$ eV, $\eta = 0.36$ ($S_N \rightarrow TT_1$). Precise

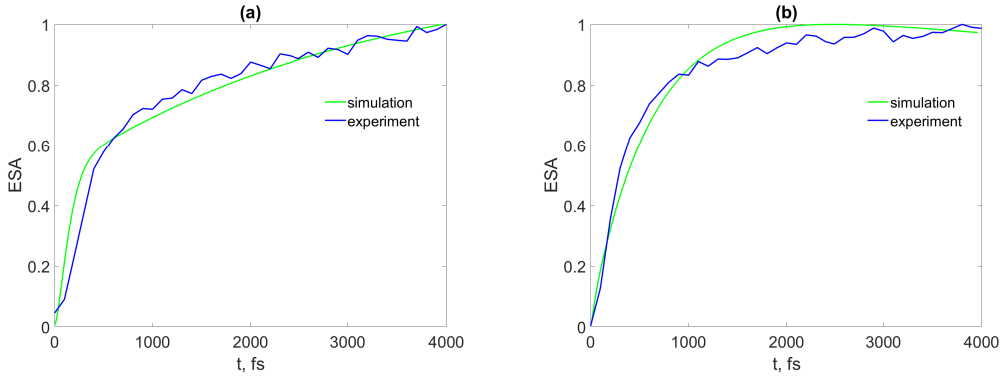

Figure 4: TA PP signals $I_{PP}(t,\omega)$ of rubrene crystal at $\omega = 2.43$ eV for the $S_1 \to TT_1$ ($\omega_{pu} = 3.1$ eV, panel (a)) and $S_N \to TT_1$ ($\omega_{pu} = 4.96$ eV, panel (b)) SF.

values of the TDM couplings are irrelevant because ESA contributions to the TA PP signals monitoring the $S_1 \to TT_1$ and $S_N \to TT_1$ SF are simply proportional to $\mu^2_{S_0S_1}\mu^2_{TT_1TT_M}$ and $\mu^2_{S_0S_N}\mu^2_{TT_1TT_M}$, respectively.

The results are presented in Fig. 4 for $S_1 \to TT_1$ ($\omega_{pu} = 3.1$ eV, panel (a)) and $S_N \to TT_1$ ($\omega_{pu} = 4.96$ eV, panel (b)) signals. Both signals exhibit two-stage kinetics with a fast ~ 1 ps rise and subsequent slower increase. However, the signal in panel (a) is raised much slower and its second-stage kinetics is much more pronounced. These behaviors correlate with two-stage evolutions of the SF populations in Fig. 2 and can be rationalized as follows. For $S_1 \to TT_1$ SF, the energy gap $\Delta_E \approx 0$ and $\Delta_E/\Omega \approx 0$. For $S_N \to TT_1$ SF, $\Delta_E \approx 2.36$ eV and $\Delta_E/\Omega \approx 12.7$. Hence vibrational levels are perfectly aligned in the $S_1 \to TT_1$ process, while alignment is rather poor for $S_N \to TT_1$. Following the analysis of Fig. 2(c), one could prematurely conclude that the $S_1 \to TT_1$ SF should be faster. However, the level-alignment argument is not applicable to the $S_N \to TT_1$ SF system, because it operates in the large energy gap regime ($\Delta_E \gg \Omega$) illustrated in Fig. 2(d), where SF is fast and is primarily controlled by the ballistic downhill wavepacket motion. Furthermore, the values of the coupling coefficients $U_{S_1TT_1}$ and $U_{S_NTT_1}$ are quite similar. Hence the fast $S_N \to TT_1$ SF is caused by the stronger coupling to the environment, which is quantified by the relaxation parameters η (see Fig. 2(b)). Much stronger impact of the environment on the $S_N \to TT_1$ SF is caused by much higher density of upper-lying electronic states.

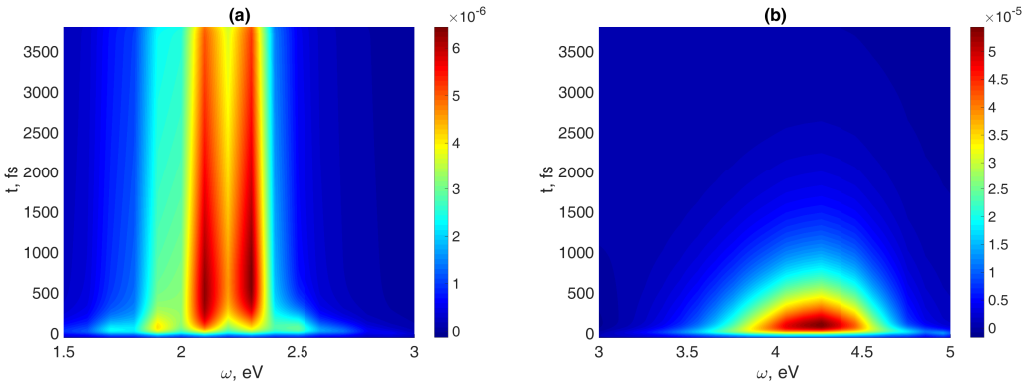

Figure 5: TFRL spectra $I_{LU}(t,\omega)$ simulated for the $S_1 \rightarrow TT_1$ (a) and $S_N \rightarrow TT_1$ (b) SF of rubrene.

Finally, the TFRL spectra $I_{LU}(t,\omega)$ simulated for the $S_1 \rightarrow TT_1$ and $S_N \rightarrow TT_1$ systems of Fig. 4 are shown, respectively, in Fig. 5(a) and (b). $I_{LU}(t,\omega)$ in panel (a) exhibits a fast rise around $t = 0$ followed by a picosecond decay. In the frequency domain, the spectrum features two pronounced vibrational lines around $\omega = 2.1$ and 2.286 eV, revealing two strongest Franck-Condon transitions. In the time domain, vibrational effects cannot be resolved since the up-conversion time resolution of 50 fs exceeds the vibrational period period of $\tau^{\Omega} = 22$ fs (see Ref.[74] for discussion of these effects). Qualitatively, the TFRL spectrum in Fig. 5(a) reminds the spectra in panels (e) and (f) of Fig. 3 after $t > 300$ fs. The TFRL spectrum in Fig. 5(b) reveals the S_N lifetime, decays almost to zero on a ~ 1 ps timescale and resembles the spectrum in Fig. 3(d).

In summary, we theoretically study the SF processes triggered in upper singlet states and develop computational methodology for the simulation of laser-induced population dynamics as well as TA PP and TFRL spectra revealing the $S_1 \rightarrow TT_1$ and $S_N \rightarrow TT_1$ SF. With this methodology, any number of relevant singlet, triplet, and charge-transfer states can be treated and, if necessary, electronic two-dimensional or six-wave-mixing signals can be simulated by employing the methods outlined in Refs.[75,76] For clarity, exciton-exciton annihilation is not considered, but can readily be included in simulations following, e. g., the methodology of Ref.[77]

We demonstrate that SF from upper singlet states can be fast and efficient, since the molecular wavepacket launched to the upper state S_N from the ground state S_0 by the pump pulse is usually located above the crossing of the $S_N - TT_1$ PESs. This promotes the downhill ballistic wavepacket

motion and facilitates the $S_N \rightarrow TT_1$ SF. Temperature effects are of minor importance in this case, because the initial placement of the wavepacket in the S_N PES is primarily determined by the carrier frequency of the pump pulse. Reaction pathways leading to the $S_N \rightarrow TT_1$ SF are usually much more diverse than those responsible for the $S_1 \rightarrow TT_1$ SF, owing to the high density of upper singlet states and rich structure of their PESs landscapes. This creates new opportunities for optimizing the $S_N \rightarrow TT_1$ SF, either through chemical modifications of the SF materials or by employing various laser control techniques. In particular, the direct $S_N \rightarrow TT_1$ SF can coexist with the sequential $S_N \rightarrow S_M \rightarrow S_1 \rightarrow TT_1$ SF, and interference of these two pathways can be exploited for maximizing the SF yield.

Nowadays, SF is under active lab studies but is still quite far from industrial applications.[78–80] Researchers are therefore looking for additional venues of controlling and enhancing SF. Apart from the search for different molecular materials suitable for SF,[3,6] micro cavities are widely used for engineering SF systems (see reviews[81–83] as well as recent theoretical[84–86] and experimental[87,88] works). The present study demonstrates that SF from upper singlet states may be used as an alternative, technically simpler and more robust practical method for manipulating, optimizing, and controlling SF. Along with bias voltage[89] and temperature,[10,90,91] the carrier frequency of the pump pulse is a reliable and efficient parameter governing the SF process (see Ref.[92] and Refs.[11–17] for probing lower- and upper-lying electronic states, respectively). The pump pulse intensity can also be harnessed for SF manipulation,[93,94] and we will explore this scenario in our future studies.

The title of the present work is a paraphrase of the seminal Feynman's *Plenty of Room at the Bottom* – the motto which triggered the nanoscience development. We are convinced that there is plenty of room on the top, and SF from upper singlet states should be further studied and exploited. After all, the solar spectrum is broad and its blue wing shoots above lowest excited states of most of molecular materials. From this perspective, the $S_N \rightarrow TT_1$ SF is a general mechanism and promising scenario for solar harvesting applications.

Acknowledgments

M. F. G. acknowledges support of Hangzhou Dianzi University through startup funding.

References

(1) Singh, S.; Jones, W. J.; Siebrand, W.; Stoicheff, B. P.; Schneider, W. G. Laser Generation of Excitons and Fluorescence in Anthracene Crystals. *J. Chem. Phys.* **1965**, *42*, 330.

(2) Smith, M. B.; Michl, J. Singlet Fission. *Chem. Rev.* **2010**, *110*, 6891-6936.

(3) Japahuge, A.; Zeng, T. Theoretical Studies of Singlet Fission: Searching for Materials and Exploring Mechanisms. *ChemPlusChem* **2018**, *83*, 146-182.

(4) Miyata, K.; Conrad-Burton, F. S.; Geyer, F. L.; Zhu, X.-Y. Triplet Pair States in Singlet Fission. *Chem. Rev.* **2019**, *119*, 4261-4292.

(5) Reichman, D. R.; Zhu, X. Singlet Fission. *J. Chem. Phys.* **2020**, *153*, 110401.

(6) Ullrich, T.; Munz, D.; Guldi, D. M. Unconventional Singlet Fission Materials. *Chem. Soc. Rev.* **2021**, *50*, 3485.

(7) Bardeen, C. J. Time dependent Correlations of Entangled States with Nondegenerate Branches and Possible Experimental Realization Using Singlet Fission. *J. Chem. Phys.* **2019**, *151*, 124503.

(8) Shockley, W.; Queisser, H. J. Detailed Balance Limit of Efficiency of p-n Junction Solar Cells. J. Appl. Phys. **1961**, 32, 510.

(9) Markvart, T. Shockley: Queisser Detailed Balance Limit After 60 Years. WIREs Energy Environ. **2022**, e430.

(10) Miyata, K.; Kurashige, Y.; Watanabe, K.; Sugimoto, T.; Takahashi S.; Tanaka S.; Takeya, J.; Yanai, T; Matsumoto, Y. Coherent Singlet Fission Activated by Symmetry Breaking. *Nat. Chem.* **2017**, *9*, 983-989.

(11) Ma, L.; Zhang, K.; Kloc, C.; Sun, H.; Michel-Beyerle, M. E.; Gurzadyan, G. G. Singlet Fission in Rubrene Single Crystal: Direct Observation by Femtosecond Pump-Probe Spectroscopy. *Phys. Chem. Chem. Phys.* **2012**, *14*, 8307-8312.

(12) Ma, L.; Zhang, K.; Kloc, C.; Sun, H.; Soci, C.; Michel-Beyerle, M. E.; Gurzadyan, G. G. Fluorescence From Rubrene Single Crystals: Interplay of Singlet Fission and Energy Trapping. Phys. Rev. B **2013**, 87, 201203(R).

(13) Wu, T.; Ni, W.; Gurzadyan, G. G.; Sun, L. Singlet Fission From Upper Excited Singlet States and Polaron Formation in Rubrene Film. *RSC Adv.* **2021**, *11*, 4639.

(14) Ni, W.; Gurzadyan, G. G.; Zhao, J.; Che, Y.; Li, X.; Sun, L. Singlet Fission from Upper Excited Electronic States of Cofacial Perylene Dimer. *J. Phys. Chem. Lett.* **2019**, 10, 2428-2433.

(15) Ni, W.; Gurzadyan, G. G.; Ma, L.; Hu, P.; Kloc, C.; Sun, L. Ultrafast Tuning of Various Photochemical Pathways in Perylene-TCNQ Charge-Transfer Crystals. *J. Phys. Chem. C* **2020**, *124*, 13894-13901.

(16) Ni, W.; Sun, L.; Gurzadyan, G. G. Ultrafast Spectroscopy Reveals Singlet Fission, Ionization and Excimer Formation in Perylene Film. *Sci. Rep.* **2021**, *11*, 5220.

(17) Zhao, T.; Kloc, C.; Ni, W.; Sun, L.; Gurzadyan, G. G. Revealing Ultrafast Relaxation Dynamics in Six-thiophene Thin Film and Single Crystal. *J. Photochem. Photobiol. A* **2021**, 404, 112920.

(18) Bakulin, A. A.; Morgan, S. E.; Kehoe, T. B.; Wilson, M. W. B.; Chin, A. W.; Zigmantas,

D.; Egorova, D.; Rao, A. Real-Time Observation of Multiexcitonic States in Ultrafast Singlet Fission Using Coherent 2D Electronic Spectroscopy. *Nat. Chem.* **2016**, *8*, 16-23.

(19) Tempelaar, R.; Reichman, D. R. Vibronic Exciton Theory of Singlet Fission. I. Linear Absorption and the Anatomy of the Correlated Triplet Pair State. *J. Chem. Phys.* **2017**, *146*, 174703.

(20) Tempelaar, R.; Reichman, D. R. Vibronic Exciton Theory of Singlet Fission. II. Two-Dimensional Spectroscopic Detection of the Correlated Triplet Pair State. *J. Chem. Phys.* **2017**, *146*, 146, 174704.

(21) Tempelaar, R.; Reichman, D. R. Vibronic Exciton Theory of Singlet Fission. III. How Vibronic Coupling and Thermodynamics Promote Rapid Triplet Generation in Pentacene Crystals. *J. Chem. Phys.* **2018**, *148*, 244701.

(22) Burdett, J. J.; Bardeen, C. J. Quantum Beats in Crystalline Tetracene Delayed Fluorescence Due to Triplet Pair Coherences Produced by Direct Singlet Fission. *J. Am. Chem. Soc.* **2012**, *134*, 8597-8607.

(23) Piland, G. B.; Burdett, J. J.; Dillon, R. J.; Bardeen, C. J. Singlet Fission: From Coherences to Kinetics. *J. Phys. Chem. Lett.* **2014**, *5*, 2312-2319.

(24) Herz, J.; Buckup,T.; Paulus, F.; Engelhart, J. U.; Bunz, U. H. F.; Motzkus, M. Unveiling Singlet Fission Mediating States in TIPS-pentacene and its Aza Derivatives. *J. Phys. Chem. A* **2015**, *119*, 6602-6610.

(25) Zhu, T.; Wan, Y.; Guo, Z.; Johnson, J.; Huang, L. Two Birds with One Stone: Tailoring Singlet Fission for Both Triplet Yield and Exciton Diffusion Length. *Adv. Mat.* **2016**, *28*, 7539-7547.

(26) Sun, K. W.; Yao, Y. Beating maps of singlet fission: Simulation of coherent two-dimensional

electronic spectroscopy by Davydov ansatz in organic molecules. *J. Chem. Phys.* **2017**, *147*, 224905.

(27) Sun, K. W.; Huang, Z. K.; Gelin, M. F.; Chen, L. P.; Zhao, Y. Monitoring of singlet fission via two-dimensional photon-echo and transient-absorption spectroscopy: Simulations by multiple Davydov trial states. *J. Chem. Phys.* **2019** *151*, 114102.

(28) Sun, K. W.; Xu, Q.; Chen, L. P.; Gelin, M. F.; Zhao, Y. Temperature effects on singlet fission dynamics mediated by a conical intersection. *J. Chem. Phys.* **2020**, *153*, 194106.

(29) Chen, L.; Borrelli, R.; Shalashilin, D. V.; Zhao, Y; Gelin, M. F. Simulation of Time-and Frequency-Resolved Four-Wave-Mixing Signals at Finite Temperatures: A Thermo-Field Dynamics Approach. *J. Chem. Theory Comput.* **2021**, *17*, 4359-4373.

(30) Hu, W.; Sun, K.; Xu, Q.; Chen, L.; Zhao, Y. Ultrafast Dynamics in Rubrene and its Spectroscopic Manifestation. *J. Chem. Phys.* **2020**, *153*, 174105.

(31) Sun, K.; Liu, X.; Hu, W.; Zhang, M.; Longd, G.; Zhao, Y. Singlet Fission Dynamics and Optical Spectra of Pentacene and its Derivatives. *Phys. Chem. Chem. Phys.* **2021**, *23*, 12654.

(32) Khan, S.; Mazumdar, S. Theory of Transient Excited State Absorptions in Pentacene and Derivatives: Triplet-Triplet Biexciton versus Free Triplets. *J. Phys. Chem. Lett.* **2017**, *8*, 5943-5948.

(33) Khan, S.; Mazumdar, S. Diagrammatic Exciton Basis Theory of the Photophysics of Pentacene Dimers. *J. Phys. Chem. Lett.* **2017**, *8*, 4468-4478.

(34) Khan, S.; Mazumdar, S. Optical Probes of the Quantum-Entangled Triplet-Triplet State in a Heteroacene Dimer. *Phys. Rev. B* **2018**, *98*, 165202.

(35) Chesler, R.; Khan, S.; Mazumdar, S. Wave Function Based Analysis of Dynamics versus Yield of Free Triplets in Intramolecular Singlet Fission. *J. Phys. Chem. A* **2020**, *124*, 10091-10099.

(36) Han, J.; Rehn, D. R.; Buckup, T.; Dreuw, A. Evaluation of Single-Reference DFT-Based Approaches for the Calculation of Spectroscopic Signatures of Excited States Involved in Singlet Fission. *J. Phys. Chem. A* **2020**, *124*, 8446-8460.

(37) Andrzejak, M.; Mazur, G.; Skora, T.; Petelenz, P. Soft Selection Rules for Femtosecond Pump-Probe Vibrational Coherence Spectroscopy. *J. Phys. Chem. C* **2020**, 124, 23501-23510.

(38) Finton, D. M.; Wolf, E. A.; Zoutenbier, V. S.; Ward, K. A.; Biaggio, I. Routes to Singlet Exciton Fission in Rubrene Crystals and Amorphous Films. *AIP Adv.* **2019**, *9*, 095027.

(39) Liu, S.; Wu, H.; Zhang, X.; Hu, W. Research Progress of Rubrene as an Excellent Multifunctional Organic Semiconductor. *Front. Phys.* **2021**, *16(1)*, 13304.

(40) Renger, T.; May, V.; Kuhn, O. Ultrafast Excitation Energy Transfer Dynamics in Photosynthetic Pigment-Protein Complexes. *Phys. Rep.* **2001**, *343*, 137-254.

(41) Gelin, M. F.; Egorova, D.; Domcke, W. A New Method for the Calculation of Two-Pulse Time- and Frequency-Resolved Spectra. *Chem. Phys.* **2005**, *312*, 135-143.

(42) Palacino-Gonzalez, E.; Gelin, M. F.; Domcke, W. Analysis of Transient-Absorption Pump-Probe Signals of Nonadiabatic Dissipative Systems: "Ideal" and "real" Spectra. *J. Chem. Phys.* **2019**, *150*, 204102.

(43) Koppel, H.; Domcke, W.; Cederbaum, L. S. Multimode Molecular Dynamics Beyond the Born-Oppenheimer Approximation. *Adv. Chem. Phys.* **1984**, *57*, 59.

(44) Domcke, W; Stock, G. Theory of Ultrafast Nonadiabatic Excited-State Processes and their Spectroscopic Detection in Real Time. Adv. Chem. Phys. **1997**, 100, 1-169.

(45) Hestand, N. J. and Spano, F. C. Expanded Theory of H- and J- Molecular Aggregates: The Effects of Vibronic Coupling and Intermolecular Charge Transfer. *Chem. Rev.* **2018**, *118*, 7069-7163.

(46) Oberhofer, H.; Reuter, K.; Blumberger, J. Charge Transport in Molecular Materials: An Assessment of Computational Methods. *Chem. Rev.* **2017**, *117*, 10319–10357.

(47) Tamura, H.; Huix-Rotllant, M.; Burghardt, I.; Olivier, Y.; Beljonne, D. First-Principles Quantum Dynamics of Singlet Fission: Coherent versus Thermally Activated Mechanisms Governed by Molecular π Stacking. *Phys. Rev. Lett.* **2015**, *115*, 107401.

(48) Renaud, N.; Grozema, F. C. Intermolecular Vibrational Modes Speed Up Singlet Fission in Perylenediimide Crystals. *J. Phys. Chem. Lett.* **2015**, *6*, 360-365.

(49) Zang, H.; Zhao, Y.; Liang, W. Z. Quantum Interference in Singlet Fission: J- and H-Aggregate Behavior. *J. Phys. Chem. Lett.* **2017**, *8*, 5105-5112.

(50) Reddy, S. R.; Coto, P. B.; Thoss, M. Quantum Dynamical Simulation of Intramolecular Singlet Fission in Covalently Coupled Pentacene Dimers. *J. Chem. Phys.* **2019**, *151*, 044307.

(51) Xie, X.; Santana-Bonilla, A.; Fang, W.; Liu, C.; Troisi, A.; Ma, H. Exciton-Phonon Interaction Model for Singlet Fission in Prototypical Molecular Crystals. *J. Chem. Theory Comput.* **2019**, *15*, 3721-3729.

(52) Gelin, M. F.; Borrelli, R.; Domcke, W. Efficient orientational averaging of nonlinear optical signals in multi-chromophore systems. *J. Chem. Phys*. **2017**, *147*, 044114.

(53) Redfield, A. G. On the Theory of Relaxation Processes. *IBM J. Res. Dev*. **1957**, 1, 19.

(54) *Pollard*, W. T.; Friesner, R. A. Solution of the Redfield Equation for the Dissipative Quantum Dynamics of Multilevel Systems. *J. Chem. Phys.* **1994**, *100*, 5054.

(55) Egorova, D.; Thoss, M.; Domcke, W.; Wang, H. Modeling of Ultrafast Electron-Transfer Processes: Validity of Multilevel Redfield Theory. *J. Chem. Phys.* **2003**, *119*, 2761.

(56) Egorova, D.; Gelin, M. F.; Thoss, M.; Wang, H.; Domcke, W. Effects of Intense Femtosecond Pumping on Ultrafast Electronic-Vibrational Dynamics in Molecular Systems with Relaxation. *J. Chem. Phys*. **2008**, *129*, 214303.

(57) Li, X.; Gurzadyan, G. G.; Gelin, Maxim F.; Domcke, W.; Gong, C.; Liu, J.; Sun, L. Enhanced S_2 Fluorescence from a Free-Base Tetraphenylporphyrin Surface-Mounted Metal Organic Framework. *J. Phys. Chem. C* **2018**, *122*, 23321-23328.

(58) Ni, W.; Gurzadyan, G. G.; Sun, L.; Gelin, M. F. Toward Efficient Photochemistry from Upper Excited Electronic States: Detection of Long S_2 Lifetime of Perylene. *J. Chem. Phys.* **2021**, *155*, 191102.

(59) Musser, A. J.; Liebel, M.; Schnedermann, C.; Wende, T.; Kehoe, T. B.; Rao, A.; Kukura, P. Evidence for Conical Intersection Dynamics Mediating Ultrafast Singlet Exciton Fission. *Nat. Phys.* **2015**, *11*, 352-357.

(60) Morrison, A. F.; Herbert, J. M. Evidence for Singlet Fission Driven by Vibronic Coherence in Crystalline Tetracene. *J. Phys. Chem. Lett.* **2017**, *8*, 1442-1448.

(61) Duan, H.-G.; Jha, A.; Li, X.; Tiwari, V.; Ye, H.; Nayak, P. K.; Zhu, X.-L.; Li, Z.; Martinez, T. J.; Thorwart, M.; Miller, R. J. D. Intermolecular Vibrations Mediate Ultrafast Singlet Fission. *Sci. Adv.* **2020**, *6*, eabb0052.

(62) Wang, G.; Zhang, C.; Liu, Z.; Wang, R.; Ma, H.; Wang, X.; Xiao, M. Singlet Fission Dynamics in Tetracene Single Crystals Probed by Polarization-Dependent Two-Dimensional Electronic Spectroscopy. *J. Phys. Chem. A* **2020**, *124*, 10447-10456.

(63) Seiler, H.; Krynski, M.; Zahn, D.; Hammer, S.; Windsor, Y. W.; Vasileiadis, T.; Pflaum, J.; Ernstorfer, R.; Rossi, M.; Schwoerer, H. Nuclear Dynamics of Singlet Exciton Fission in Pentacene Single Crystals. *Sci. Adv.* **2021**, *7*, eabg0869.

(64) Schultz, D. J. D.; Shin, J. Y.; Chen, M.; O'Connor, J. P.; Young, R. M.; Ratner, M. A.; Wasielewski, M. R. Influence of Vibronic Coupling on Ultrafast Singlet Fission in a Linear Terrylenediimide. *J. Am. Chem. Soc.* **2021**, *143*, 2049-2058.

(65) Kim, W.; Musser, A. J.Tracking Ultrafast Reactions in Organic Materials Through Vibrational Coherence: Vibronic Coupling Mechanisms in Singlet Fission. *Adv. Phys.* X, **2021**, *6*, 1918022.

(66) Generic Aspects of the Dynamics at Conical Intersections: Internal Conversion, Vibrational Relaxation and Photoisomerization 395 W. Domcke, In W. Domcke, D. Yarkony, H. Koppel (Eds.). *Conical Intersections: Dynamics, Electronic Structure, and Spectroscopy*; World Scientific, Singapore, 2004. PP 395-428.

(67) Doria, S.; Di Donato, M.; Borrelli, R.; Gelin, M. F.; Caram, J.; Pagliai, M.; Foggi, P.; Lapini, A. Vibronic Coherences in Light Harvesting Nanotubes: Unraveling the Role of Dark States. *J. Mater. Chem. C* **2022**, *10*, 7216-7226.

(68) Bixon, M.; Jortner, J. Electron Transfer-from Isolated Molecules to Biomolecules. *Adv. Chem. Phys.* **2007**, 35-202.

(69) Jang, S. J. A Simple Generalization of the Energy Gap Law for Nonradiative Processes. *J. Chem. Phys.* **2021**, *155*, 164106.

(70) Demchenko, A. P.; Tomin, V. I.; Chou, P. T. Breaking the Kasha Rule for More Efficient Photochemistry. *Chem. Rev.* **2017**, *117*, 13353-13381.

(71) Shapiro, M.; Brumer, P. Coherent Control of Molecular Dynamics. *Rep. Prog. Phys.* **2003**, *66*, 859-942.

(72) Parenti, K. R.; Chesler, R.; He, G.; Bhattacharyya, P.; Xiao, B.; Malinowski, D.; Zhang, J.; Yin, X.; Shukla, A.; Mazumdar, S.; Sfeir, M. Y.; Campos, L. M. The Role of Quantum Interference in Intramolecular Singlet Fission. **2022**, https://doi.org/10.26434/chemrxiv-2022-20qd5

(73) Ma,L.; Galstyan, G.; Zhang, K.; Kloc, C.; Sun, H.; Soci, S.; Michel-Beyerle, M. E.;

Gurzadyan, G. G. Two-Photon-Induced Singlet Fission in Rubrene Single Crystal. *J. Chem. Phys.* **2013**, *138*, 184508.

(74) Egorova, D.; Gelin, M. F.; Domcke, W. Time- and frequency-resolved luminescence spectra of nonadiabatic dissipative systems: What photons can tell us. *J. Chem. Phys.* **2005**, *122*, 134504.

(75) Gelin, M. F., Egorova, D.; Domcke, W. Efficient Calculation of Time- and Frequency-Resolved Four-Wave-Mixing Signals. *Acc. Chem. Res.* **2009**, *42*, 1290-1298.

(76) Gelin, M. F.; Egorova, D.; Domcke, W. Efficient Calculation of the Polarization Induced by N Coherent Laser Pulses. *J. Chem. Phys.* **2009**, *131*, 194103.

(77) May, V. Kinetic Theory of Exciton-Exciton Annihilation. *J. Chem. Phys.* **2014**, *140*, 054103..

(78) Daiber, B.; van den Hoven, K.; Futscher, M. H.; Ehrler, B. Realistic Efficiency Limits for Singlet-Fission Silicon Solar Cells. *ACS Energy Lett.* **2021**, *6*, 2800-2808.

(79) Baldacchino, A. J.; Collins, M. I.; Nielsen, M. P.; Schmidt, T. W.; McCamey, D. R.; Tayebjee, M. J. Y. Singlet Fission Photovoltaics: Progress and Promising Pathways. *Chem. Phys. Rev.* **2022**, *3*, 021304.

(80) Hudson, R. J.; Stuart, A. N.; Huang, D. M.; Kee, T. W. What Next for Singlet Fission in Photovoltaics? The Fate of Triplet and Triplet-Pair Excitons. *J. Phys. Chem. C* **2022**, *126*, 5369-5377.

(81) Du, M.; Ribeiro, R. F.; Yuen-Zhou, J. Remote Control of Chemistry in Optical Cavities. *Chem.* **2019**, *5*, 1167-1181.

(82) Polak, D.; Jayaprakash, R.; Lyons, T. P.; Martınez-Martınez, L. A.; Leventis, A.; Fallon, K. J.; Coulthard, H.; Bossanyi, D. G.; Georgiou, K.; Petty, A. J.; Anthony, J.; Bronstein, H.; Yuen-Zhou, J.; Tartakovskii, A. I.; Clark, J.; Musser, A. J. Manipulating Molecules with

Strong Coupling: Harvesting Triplet Excitons in Organic Exciton Microcavities. *Chem. Sci.* **2020**, *11*, 343.

(83) Gu, B.; Mukamel, S. Manipulating Nonadiabatic Conical Intersection Dynamics by Optical Cavities. *Chem. Sci.* **2020**, *11*, 1290.

(84) Gu, B.; Mukamel, S. Optical-Cavity Manipulation of Conical Intersections and Singlet Fission in Pentacene Dimers. *J. Phys. Chem. Lett.* **2021**, *12*, 2052-2056.

(85) Sun, K.; Gelin, M. F.; Zhao, Y. Accurate Simulation of Spectroscopic Signatures of Cavity-Assisted, Conical-Intersection-Controlled Singlet Fission Processes. *J. Phys. Chem. Lett.* **2022**, *13*, 4280-4288.

(86) Sun, K.; Gelin, M. F.; Zhao, Y. Engineering Cavity Singlet Fission in Rubrene. *J. Phys. Chem. Lett.* **2022**, *13*, 4090-4097.

(87) Takahashi, S.; Watanabe, K.; Matsumoto, Y. Singlet Fission of Amorphous Rubrene Modulated by Polariton Formation. *J. Chem. Phys.* **2019**, 151, 074703.

(88) Liu, B.; Menon, V. M.; Sfeir, M. Y. Ultrafast Thermal Modification of Strong Coupling in an Organic Microcavity. *APL Photon.* **2021**, *6*, 016103.

(89) Tang, X.; Hu, Y.; Jia, W.; Pan, R.; Deng, J.; Deng, J.; He, Z.; Xiong, Z. Intersystem Crossing and Triplet Fusion in Singlet-Fission- Dominated Rubrene-Based OLEDs Under High Bias Current. *ACS Appl. Mater. & Interf.* **2018**, *10*, 1948-1956.

(90) Li, J.; Chen, Z.; Zhang, Q.; Xiong, Z.; Zhang, Y. Temperature-Dependent Singlet Exciton Fission Observed in Amorphous Rubrene Films. *Org. Electr.* **2015**, *26*, 213-217.

(91) Zhao, D. X.; O'Connor, J. P.; Schultz, J. D.; Bae, Y. J.; Lin, C.; Young, R. M.; Wasielewski, M. R. Temperature Tuning of Coherent Mixing between States Driving Singlet Fission in a Spiro-Fused Terrylenediimide. *J. Phys. Chem. B* **2021**, *125*, 6945-6954.

(92) Wilson, M. W. B.; Rao, A.; Clark, J.; Kumar, R. S. S.; Brida, D.; Cerullo, G.; Friend, R. H. Ultrafast Dynamics of Exciton Fission in Polycrystalline Pentacene. *J. Am. Chem. Soc.* **2011**, *133*, 11830-11833.

(93) Ishibashi, Y.; Inouea, Y.; Asahi, T. The Excitation Intensity Dependence of Singlet Fission Dynamics of a Rubrene Microcrystal Studied by Femtosecond Transient Microspectroscopy. *Photochem. Photobiol. Sci.* **2016**, *15*, 1304-1309.

(94) Cruz, C. D.; Choi, H. H; Podzorov, V.; Chronister, E. L.; Bardeen, C. J. Photon Upconversion in Crystalline Rubrene: Resonant Enhancement by an Interband State. *J. Phys. Chem. C* **2018**, *122*, 17632-17642.